ISSN 0036-0295, Russian Metallurgy (Metally), Vol. 2022, No. 5, pp. 512–519. © Pleiades Publishing, Ltd., 2022.
Russian Text © The Author(s), 2022, published in Metally, 2022, No. 3, pp. 56–64.

Effect of Rotary Swaging and Subsequent Aging on the Structure and Mechanical Properties of a Cu–0.5% Cr–0.08% Zr Alloy

N. S. Martynenko[a, *], N. R. Bochvar[a], O. V. Rybalchenko[a], A. I. Bodyakova[b, c], M. M. Morozov[a], N. P. Leonova[a], V. S. Yusupov[a], and S. V. Dobatkin[a, c]

[a] *Baikov Institute of Metallurgy and Materials Science, Russian Academy of Sciences, Moscow, Russia*
[b] *Belgorod State University, Belgorod, Russia*
[c] *National University of Science and Technology MISiS, Moscow, Russia*
**e-mail: nmartynenko@imet.ac.ru*

Received December 22, 2021; revised February 18, 2022; accepted March 4, 2022

Abstract—The effect of rotary swaging (RS) at various strains and subsequent aging at various temperatures on the structure and the mechanical properties of a Cu–0.5% Cr–0.08% Zr alloy is studied. RS is shown to form a microstructure with grains extended along the deformation axis. The grain size decreases with increasing strain. Subgrains 300–400 nm in size and shear bands 200 nm in width are observed inside the elongated grains formed upon RS at $\varepsilon = 2.77$. Microstructural refinement significantly increases the strength of the alloy but decreases its plasticity. Subsequent aging further increases the strength and the electrical conductivity of the alloy due to the precipitation of fine chromium and Cu_5Zr-phase particles. Quenching, RS at $\varepsilon = 2.77$, and subsequent aging at 500°C for 1 h result in the best combination of strength (557 ± 18 MPa), plasticity (17.1 ± 2.6%), and electrical conductivity (83.4 ± 1.6% IACS) of the Cu–0.5%Cr–0.08%Zr alloy.

Keywords: copper alloys, rotary swaging, aging, microstructure, mechanical properties, electrical conductivity
DOI: 10.1134/S0036029522050081

INTRODUCTION

Low-alloy copper alloys can be used as electric materials due to their high thermal and electrical conductivities [1–3]. The Cu–Cr–Zr system is one of the most popular systems of electrical copper alloys [3–5]. The alloys of this system, similarly to many low-alloy copper alloys intended for electrical engineering, are precipitation-hardening alloys. Fine chromium-phase [6, 7] and Cu_5Zr-phase [4, 7–9] particles precipitate in them during aging. These particles are effective hardeners, and their precipitation depletes a copper solid solution and additionally increases the electrical conductivity. For example, aging of a Cu–0.25% Cr–0.1% Zr alloy at 490°C for 1 h was shown to increase its yield strength from 32.5 to 230 MPa due to the precipitation of ultrafine phases [4]. Aging of a Cu–0.7% Cr–0.07% Zr alloy at 475°C for 1 h increased its yield strength from 40 to 240 MPa and its tensile strength from 177 to 342 MPa and decreased the plasticity of the alloy from 51 to 32%. The electrical conductivity of the alloy increased from ~33 to ~58% IACS due to the depletion of the supersaturated solid solution [10].

However, the precipitation hardening effect is often insufficient for the successful application of low-alloy copper alloys in the electrical industry. Therefore, aging of these alloys is usually combined with their strain hardening. The latter further increases the mechanical properties of the copper alloys due to the refinement of their microstructure, which, in turn, often increases the fatigue strength and wear resistance. As was shown for a Cu–0.7% Cr–0.9% Hf alloy, equal-channel angular pressing (ECAP) and subsequent aging can increase the wear resistance of spot-welding electrodes. The relative broadening of the working electrode surface decreased by 5.3 and 3.5 times after 2×10^3 and 4×10^3 welding cycles, respectively, as compared to its initial state [11]. The grain size in a Cu–0.1% Zr alloy decreased when the number of ECAP passes was increased, which resulted in a decrease in the friction coefficient of the alloy and, as a consequence, an increase in its wear resistance [12]. Consequently, the formation of an ultrafine-grained (UFG) structure in copper alloys makes their strength and functional properties better. An UFG structure in metals and alloys is currently formed mainly by severe plastic deformation (SPD) techniques, including the above-mentioned ECAP. SPD techniques are effective for improving the strength and performance characteristics of materials, but, unfortunately, they are poorly developed for commercial applications. Therefore, the development of traditional deformation techniques aimed at forming an UFG structure in metals and alloys is a challenging problem. Rotary swaging (RS), a deformation tech-

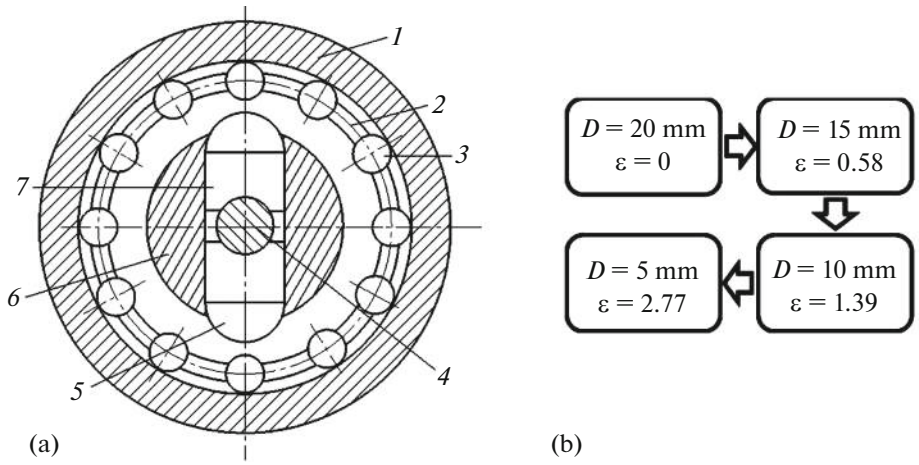

Fig. 1. (a) Schematic of the RS machine: (*1*) fixed cage, (*2*) sliding ram, (*3*) roller, (*4*) billet, (*5*) rolling die, (*6*) spindle, and (*7*) die. (b) Technological schematic of the RS process.

nique based on all-round compression and producing axially symmetric long billets, can be referred to promising techniques [13].

RS was shown to refine the microstructure of various metals and alloys, including alloys of the Cu–Cr–Zr system [14–18], up to an UFG state. RS and two-stage aging of a Cu–0.3% Cr–0.1% Zr–0.05% Mg alloy succeeded in increasing its ultimate tensile strength to 612 MPa at a relative elongation of 5% and an electrical conductivity of 84.7% IACS [18]. Therefore, RS and subsequent aging led to a good combination of strength, plasticity, and electrical conductivity of low-alloyed copper alloys. This work aims at investigating the effect of different degrees of RS deformation on the mechanical properties, the electrical conductivity, and the aging behavior of a Cu–0.5% Cr–0.08% Zr alloy.

EXPERIMENTAL

We used the Cu–0.5% Cr–0.08% Zr alloy (hereafter, the content is given in wt %) melted using Cu–5% Cr and Cu–10% Zr master alloys. They were melted from high-purity metals (99.96% Cu, 99.95% Cr, 99.8% Zr) in a pure argon atmosphere in a vacuum arc furnace on a copper water-cooled base using a nonconsumable tungsten electrode. The alloy was melted in a vacuum induction furnace in an argon atmosphere in a corundum crucible and cast into a graphite mold 50 mm in diameter and 120 mm in height also in the argon atmosphere. The alloy was homogenized at 800°C for 1 h and then air cooled. Before pressing, the alloy was additionally heated at 800°C (for ~40 min) in a furnace and the container was heated to 400°C. The resulting rod 25 mm in diameter was machined to a diameter of 20 mm required for the subsequent deformation. After pressing, the rods were annealed at 1000°C for 2 h and water quenched. RS was carried out on a RKM 2129.02 machine (at a maximum force of 8 kN) at room temperature [15]. The degree of deformation was calculated by the formula

$$\varepsilon = \ln(A_0/A_f), \quad (1)$$

where A_0 and A_f are the initial and final cross-sectional areas of the billet, respectively.

A rod of initial diameter $D = 20$ mm was used for RS. The structure, mechanical properties, and aging were investigated in the alloy deformed to total deformation degrees of 0.58, 1.39, and 2.77. For this investigation, reference samples 10 cm long were cut from the rod deformed to $\varepsilon = 0.58$ and 1.39 during swaging. The schematic illustration of the setup and the technological schematic of the RS process are shown in Fig. 1.

The microstructure of the alloy in the initial state and after RS was examined using a Carl Zeiss Jena Jenavert optical microscope in a longitudinal section of deformed samples. In addition, the alloy microstructure after RS to $\varepsilon = 2.77$ was analyzed by transmission electron microscopy (TEM) on a Jeol JEM 2100 microscope (Japan) at an accelerating voltage of 200 kV. The average size of structural constituents was estimated by the random intercept method with the Image ExpertPro 3 software.

Thermal stability (time τ = const) and aging kinetics (temperature t = const) were estimated by studying the temperature and heating time dependences of the microhardness and the electrical conductivity of the alloy. Vickers microhardness was measured using a 4402MVD Instron Wolpert Wilson Instruments automatic tester at a load of 1 N (100 gf) and a holding time of 10 s. The electrical resistance was measured on flat samples 15 × 4.5 × 1 mm (length × width × thickness) in size with a BSZ-010-2 microhmmeter. The resultant electrical resistivity was converted into electrical conductivity and, then, the percentage of conductivity of annealed copper according to the International Annealed Copper Standard (% IACS). The tensile

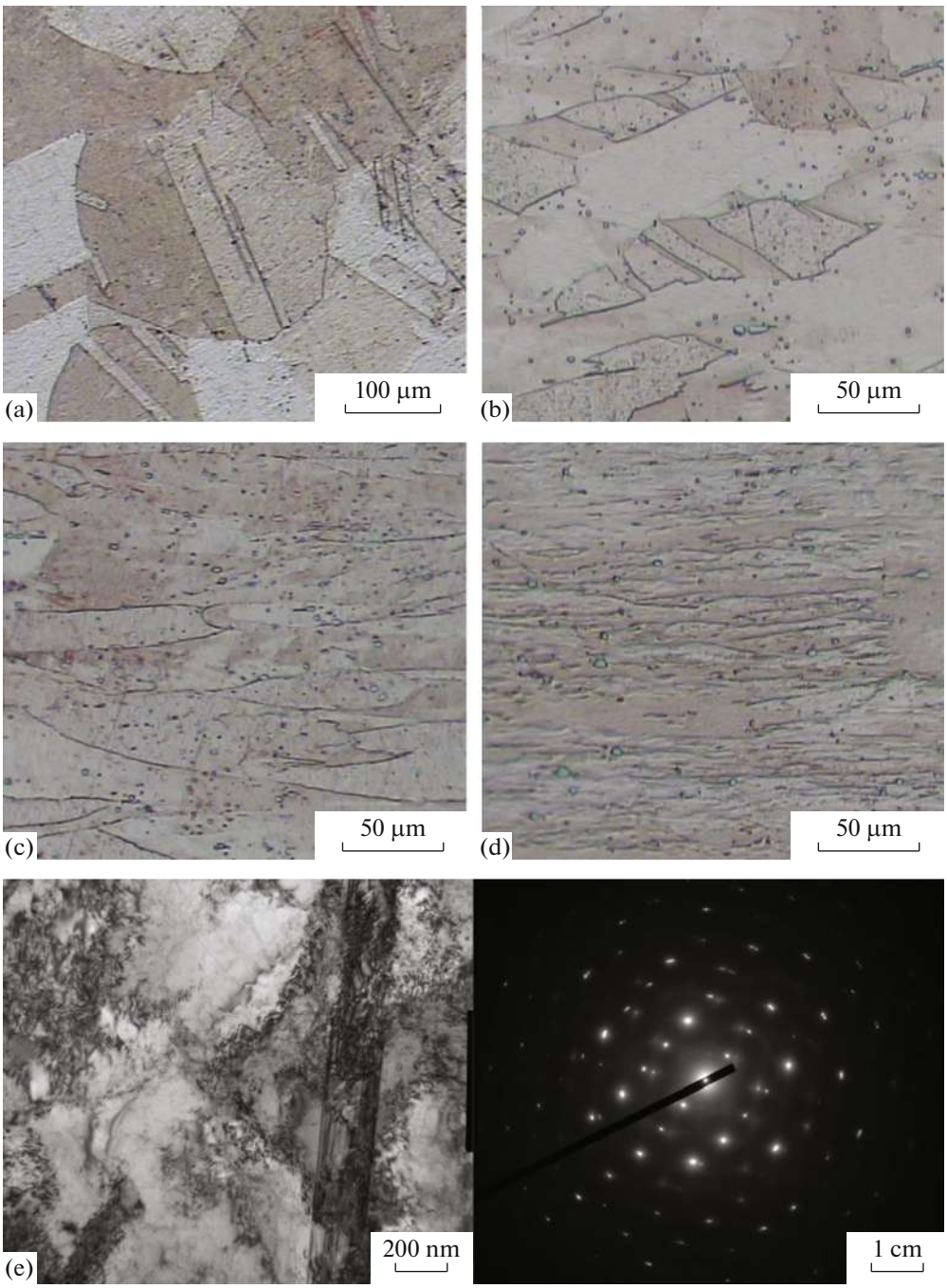

Fig. 2. Microstructure of the Cu–0.5% Cr–0.08% Zr alloy after (a) quenching and RS at (b) ε = 0.58, (c) 1.39, and (d, e) 2.77.

properties of the alloy before and after RS were measured on an Instron 3382 testing machine at room temperature. The tensile speed was 1 mm/min. Flat samples with a cross-sectional area of 2 × 1 mm and a gage length of 5.75 mm were used for the studies.

RESULTS AND DISCUSSION

Figure 2 shows the microstructure of the Cu–0.5%Cr–0.08%Zr alloy in the quenched state and after RS. The alloy structure in the quenched state consists of equiaxed grains of the supersaturated solid solution of chromium and zirconium in copper. The average grain size is 154 ± 15 μm. In addition, the structure contains annealing twins 5–10 μm wide (Fig. 1a).

RS to ε = 0.58 refines the microstructure and grains are elongated in the swaging direction (Fig. 2b). The grains are ~135 ± 12 μm in length and 67 ± 4 μm

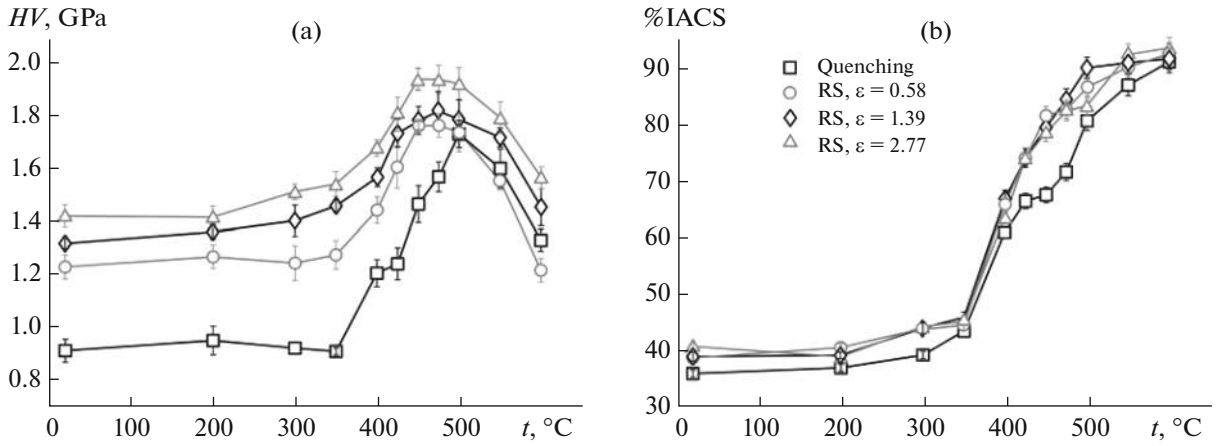

Fig. 3. Thermal stability of the Cu–0.5% Cr–0.08% Zr alloy before and after RS: (a) microhardness and (b) electrical conductivity.

in width. Similar to the quenched state, the structure contains twins 5–10 μm wide. Further RS up to ε = 1.39 leads to greater grain elongation in the deformation direction. After RS to ε = 1.39, the structure contains elongated grains with a length of several hundred micrometers and a width of 29 ± 3 μm (Fig. 2c). After RS to ε = 2.77, the alloy structure is completely banded with an average grain width of 18 ± 2 (Fig. 2d). In addition, the elongated grains exhibit an UFG structure consisting of subgrains 300–400 nm in size and bands ~200 nm in width (Fig. 2e).

Since the Cu–0.5%Cr–0.08% Zr alloy is a precipitation-hardening one, the first stage of investigation was to study its behavior during aging and to choose the optimum heat-treatment parameters (temperature, time). Therefore, we studied the thermal stability of hardening and the kinetics of aging of the alloy after quenching and the swaged initially quenched alloy. Figure 3 shows the microhardness and the electrical conductivity of the Cu–0.5% Cr–0.08% Zr alloy before and after RS as a function of the aging temperature.

RS of the alloy at room temperature was found to increase the microhardness of the alloy considerably. The greater the deformation degree, the greater the microhardness growth. The microhardness of the initial quenched alloy is 0.9 ± 0.04 GPa, whereas after RS it is 1.2 ± 0.05 GPa at ε = 0.58, 1.3 ± 0.02 GPa at ε = 1.39, and 1.4 ± 0.04 GPa at ε = 2.77. Heating in the temperature range 20–350°C for 0.5 h weakly changes the microhardness achieved after different alloy treatment processes. However, an increase in the temperature above 350°C hardens the alloy of all the studied states due to particle precipitation. The microhardness grows up to 500°C and reaches a maximum of 1.7 ± 0.05 GPa in the quenched alloy, 1.7 ± 0.07 GPa in the alloy after swaging to ε = 0.58, 1.8 ± 0.07 GPa in the alloy after swaging to ε = 1.39, and 1.9 ± 0.06 GPa in the alloy after swaging at ε = 2.77. A further increase in the temperature to 600°C softens the alloy in all states (Fig. 3a). As mentioned above, two types of particles precipitate in copper alloys containing chromium and zirconium during aging, namely, chromium particles and Cu_5Zr phase particles. The precipitation of these particles is most likely to be responsible for the alloy hardening upon aging. In addition, these particles precipitate mainly at grain boundaries, which also restrains grain growth on heating and increases the thermal stability of the alloy.

Impurity atoms (including alloying elements) are known to make the greatest contribution to the electrical resistivity, while the decomposition of a supersaturated solid solution increases the electrical conductivity of an alloy. In our case, the electrical conductivity is one of the most important service properties; therefore, we studied the electrical conductivity during aging in addition to hardening (Fig. 3b). The room-temperature studies showed a low electrical conductivity of the alloy before aging: it is 36 ± 0.6% for the quenched alloy, 39 ± 0.7% for the alloy after swaging to ε = 0.58, 39 ± 0.7% for the alloy after swaging to ε = 1.39, and 41 ± 0.7% for the alloy after swaging to ε = 2.77. Note that the electrical conductivity of the quenched alloy is slightly lower than that of the alloy after RS. This behavior can be caused by partial decomposition of a supersaturated solid solution, which occurs during swaging due to dynamic aging and results in a slight decrease in the concentration of chromium and zirconium dissolved in copper. The further behavior of the alloy on heating is in a good agreement with the results of the microhardness study. For example, the electrical conductivity of the alloy in the temperature range 20–350°C remains almost the same, which can indicate a weakly pronounced decomposition of a solid solution. A further increase in the aging temperature up to 600°C increases the electrical conductivity of the alloy mainly due to the decomposition of the supersaturated solid solution. The electrical conductivity at 500°C (microhardness maximum) is quite high and is 81 ± 1.7% for the quenched alloy, 87 ± 1.8% for the alloy after swaging

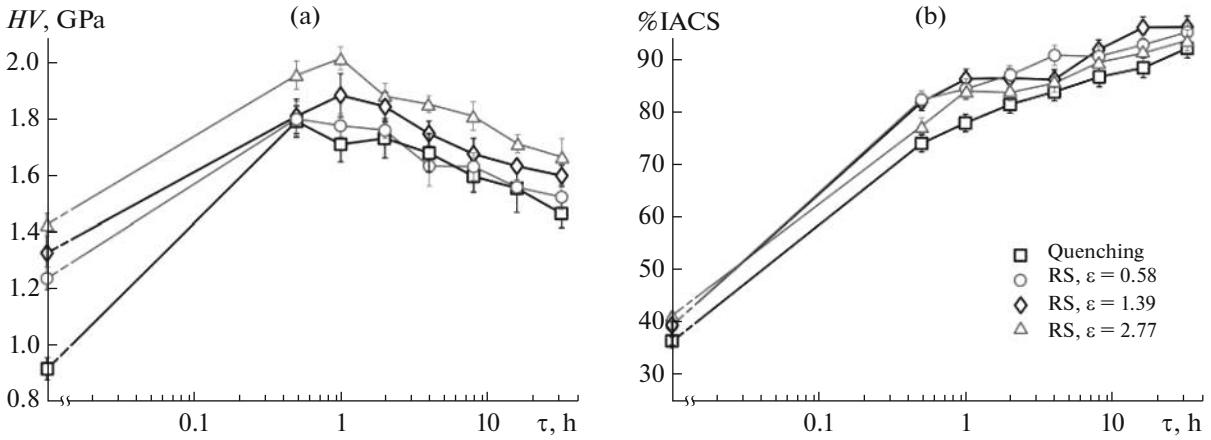

Fig. 4. Aging kinetics of the Cu–0.5% Cr–0.08% Zr alloy before and after RS: (a) microhardness and (b) electrical conductivity.

to $\varepsilon = 0.58$, 90 ± 1.9% for the alloy after swaging to $\varepsilon = 1.39$, and 84 ± 1.7% for the alloy after swaging to $\varepsilon = 2.77$.

The results of the thermal stability study were used to choose an optimal aging temperature of 500°C, at which we found the optimum combination of microhardness and electrical conductivity. The further stage of research was to study the kinetics of alloy aging in order to select the optimum aging time (Figs. 4a, 4b).

The microhardness maximum after heating at 500°C was found to be achieved in the quenched alloy after aging for 2 h and in the alloy after RS at $\varepsilon = 0.58$. The microhardness is 1.73 ± 0.07 and 1.76 ± 0.03 GPa for the quenched and swaged states, respectively. The microhardness of the alloy deformed by the RS at $\varepsilon = 1.39$ and 2.77 reaches its maximum after heating for 1 h; its values are 1.91 ± 0.08 and 2.03 ± 0.04 GPa, respectively (Fig. 4a). The time is takes for the microhardness maximum to be reached decreases with increasing strain due to the accumulation of a high density of lattice defects. These defects provide energetically favorable conditions for particle nucleation at them, increasing their number and reducing their size, which positively affects the strength. The electrical conductivity increases over the entire heating time range. However, a significant increase was observed only upon aging for 1 h, after which the increase slowed down. The electrical conductivity is 81.2 ± 1.6 and 86.7 ± 1.8% for the quenched alloy and the alloy after RS at $\varepsilon = 0.58$ and subsequent annealing for 2 h, respectively, which corresponds to the microhardness maximum. The conductivity of the alloy after RS at $\varepsilon = 1.39$ and 2.77 and aging for 1 h is 86.1 ± 1.8 and 83.4 ± 1.6%, respectively (Fig. 4b). The summary data on the microhardness and the electrical conductivity of the Cu–0.5% Cr–0.08% Zr alloy before and after RS are given in Table 1.

Figure 5 shows the microstructure of the Cu–0.5%Cr–0.08% Zr alloy after RS and subsequent aging. Similarly to the structure formed by RS, the alloy structure consists of grains elongated in the deformation direction. Additional heating increased the average grain width in the alloy deformed at $\varepsilon = 0.58$ and 1.39. After aging at 500°C for 2 h, the average grain width in the alloy swaged to $\varepsilon = 0.58$ was 79 ± 7 μm (Fig. 5a). After aging at 500°C for 1 h, the average grain width in the alloy swaged to $\varepsilon = 1.39$ was 42 ± 2 μm (Fig. 5b). Aging of the alloy swaged at $\varepsilon = 2.77$ did not change the size of elongated grains. After aging at 500°C for 1 h, the average width of elongated grains in the alloy swaged to $\varepsilon = 2.77$ was 20 ± 1 μm (Fig. 5c). The size of the subgrains formed inside these elongated grains was 400–500 nm (Fig. 5d). Furthermore,

Table 1. Microhardness and electrical conductivity (%IACS) of the Cu–0.5% Cr–0.08% Zr alloy in different states

State of alloy	Microhardness, GPa		Electrical conductivity, %IACS	
	before aging	after aging*	before aging	after aging*
Quenching	0.91 ± 0.04	1.73 ± 0.07	36.2 ± 0.7	81.2 ± 1.6
RS at $\varepsilon = 0.58$	1.23 ± 0.05	1.76 ± 0.03	39.0 ± 0.7	86.7 ± 1.8
RS at $\varepsilon = 1.39$	1.32 ± 0.02	1.91 ± 0.08	39.2 ± 0.7	86.1 ± 1.8
RS at $\varepsilon = 2.77$	1.42 ± 0.04	2.0 ± 0.04	40.9 ± 0.7	83.4 ± 1.6

* Aging at 500°C for 2 h of the quenched alloy and the alloy swaged at $\varepsilon = 0.58$ and aging at 500°C for 1 h of the alloy swaged at $\varepsilon = 1.39$ and 2.77.

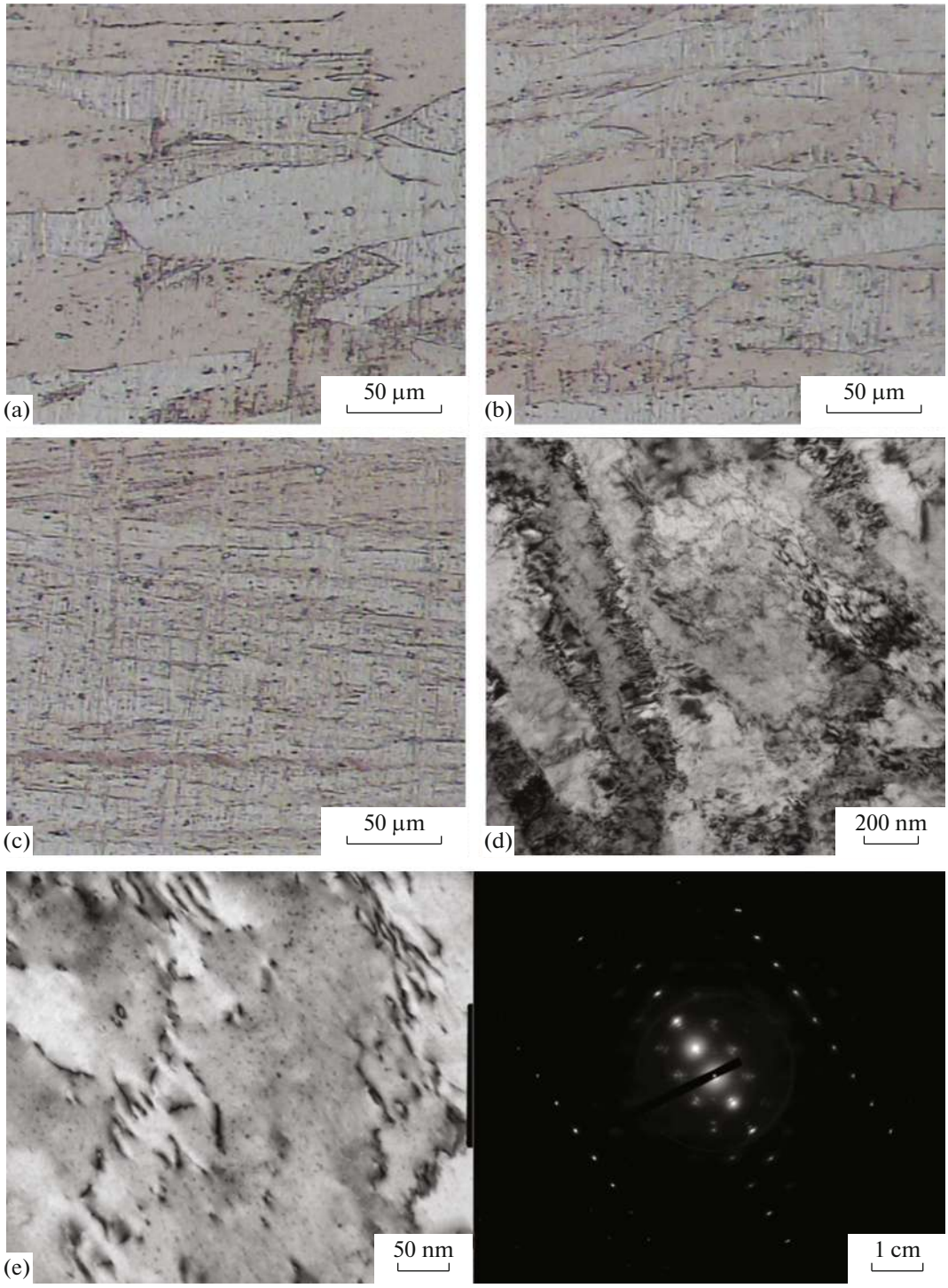

Fig. 5. Microstructure of the Cu–0.5% Cr–0.08% Zr alloy after (a) RS at ε = 0.58 and subsequent aging at 500°C for 2 h, (b) RS at ε = 1.39 and subsequent aging at 500°C for 2 h, and (c–e) RS at ε = 2.77 and subsequent aging at 500°C for 1 h.

aging at 500°C for 1 h resulted in the precipitation of fine particles several nanometers in size in the alloy swaged at ε = 2.77 (Fig. 5e). As mentioned above, these particles are most likely to be chromium [6, 7] and Cu_5Zr-phase [4, 7–9] particles.

Table 2 presents the resultant mechanical properties of the Cu–0.5% Cr–0.08% Zr alloy in the quenched state and the RS-deformed and aged states. This work shows that RS significantly increases the strength properties of the quenched alloy due to

Table 2. Mechanical properties of the Cu–0.5% Cr–0.08% Zr alloy in different states

State of alloy		$\sigma_{0.2}$	σ_u	δ, %
		MPa		
Quenching:	before aging	72 ± 4	227 ± 9	61.0 ± 1.5
	after aging	348 ± 2	442 ± 19	24.3 ± 3.2
RS at ε = 0.58:	before aging	335 ± 2	341 ± 2	20.4 ± 1.4
	after aging	404 ± 7	467 ± 10	25.4 ± 0.9
RS at ε = 1.39:	before aging	377 ± 5	380 ± 7	18.1 ± 1.0
	after aging	432 ± 10	476 ± 10	23.4 ± 3.5
RS at ε = 2.77:	before aging	426 ± 5	433 ± 5	16.2 ± 0.6
	after aging	516 ± 20	557 ± 18	17.1 ± 2.6

microstructure refinement and an increase in the lattice defect density. For example, the deformation of the quenched alloy to a degree of 0.58 increases the yield strength of the alloy from 72 ± 4 to 335 ± 2 MPa and the tensile strength from 227 ± 9 to 341 ± 2 MPa. However, the plasticity of the alloy decreases significantly from 61.0 ± 1.5% (quenched state) to 20.4 ± 1.4% (state after RS to a strain of 0.58). A further increase in the strain to 1.39 causes additional hardening of the alloy and a decrease in its plasticity. The yield strength of the alloy after RS at ε = 1.39 is 377 ± 5 MPa, and the ultimate tensile strength is 380 ± 7 MPa at a relative elongation of 18.1 ± 1.0%. The strength continues to grow in the case of RS to ε = 2.77: $\sigma_{0.2}$ increases to 426 ± 5 MPa and σ_u increases to 433 ± 5 MPa at the plasticity decreased to 16.2 ± 0.6%.

Subsequent aging of the alloy results in its additional hardening due to phase precipitation. For example, aging of the quenched alloy at 500°C for 2 h increases the ultimate tensile strength from 227 ± 9 to 442 ± 19 MPa and the yield strength from 72 ± 4 to 348 ± 2 MPa. However, the precipitation of fine phases negatively affects the plasticity: it decreases the relative elongation from 61.0 ± 1.5% in the initial state to 24.3 ± 3.2% after aging. Aging of the swaged alloy increases its strength. For example, 2-h aging of the swaged alloy (ε = 0.58) at 500°C increases its tensile strength to 467 ± 10 MPa and its yield strength to 404 ± 7 MPa and improves its plasticity (relative elongation of 25.4 ± 0.9%). Aging at 500°C for 1 h increases the ultimate tensile strength and the yield strength of the RS-deformed alloy (ε = 1.39) to 476 ± 10 and 432 ± 10 MPa, respectively, and increases plasticity from 18.1 ± 1.0 to 23.4 ± 3.5%. However, aging of the deformed alloy (ε = 2.77) at 500°C for 1 h increases its ultimate tensile strength and yield strength to 557 ± 18 and 516 ± 20 MPa, respectively, but weakly changes the plasticity of the alloy (relative elongation increases to 17.1 ± 2.6% within the limits of experimental error). The increase in the plasticity of the swaged alloy after aging can be caused by both the decomposition of the supersaturated solid solution and the heating-induced recovery processes, which decrease the density of free dislocations due to their annihilation and sinking to grain boundaries.

CONCLUSIONS

RS significantly refines the structure of the Cu–0.5% Cr–0.08% Zr alloy and forms elongated grains with an UFG submicrostructure inside them. Subsequent aging induces grain size growth and the precipitation of chromium and Cu_5Zr-phase particles.

(2) Heating of the alloy causes the decomposition of the supersaturated copper-based solid solution, increasing the strength and electrical conductivity of the alloy. The following optimum alloy aging parameters were selected based on the results of studying the decomposition: heating at 500°C for 2 h for the alloy after quenching and RS at ε = 0.58 and for 1 h for the alloy after RS at ε = 1.39 and 2.77.

(3) RS of the Cu–0.5% Cr–0.08% Zr alloy increases its strength significantly. RS at ε = 2.77 increases the ultimate tensile strength of the alloy from 227 ± 9 to 433 ± 5 MPa and the yield strength from 72 ± 4 to 426 ± 5 MPa but decreases its plasticity δ from 61.0 ± 1.5 to 16.2 ± 0.6%. Heating of the alloy at 500°C (1 h) brings about an additional increase in the strength of both the quenched alloy and the RS-deformed alloy due to the precipitation of fine particles.

(4) The best combination of the strength, ductility, and electrical conductivity was achieved by combined treatment of the Cu–0.5% Cr–0.08% Zr alloy (RS at ε = 2.77, aging at 500°C for 1 h). This treatment resulted in a tensile strength of 557 ± 18 MPa, a relative elongation of 17.1 ± 2.6%, and an electrical conductivity of 83.4 ± 1.6% IACS.

FUNDING

This work was performed within state assignment no. 075-00715-22-00.

CONFLICT OF INTEREST

The authors declare that they have no conflicts of interest.

REFERENCES

1. M. Yu. Murashkin, I. Sabirov, X. Sauvage, and R. Z. Valiev, "Nanostructured Al and Cu alloys with superior strength and electrical conductivity," J. Mater. Sci. **51**, 33–49 (2016).
2. S. Uchida, T. Kimura, T. Nakamoto, T. Ozaki, T. Miki, M. Takemura, Y. Oka, and R. Tsubota, "Microstructures and electrical and mechanical properties of Cu–Cr alloys fabricated by selective laser melting," Mater. Des. **175**, 107815 (2019).
3. Z. Shen, Z. Lin, P. Shi, J. Zhu, T. Zheng, B. Ding, Y. Guo, and Y. Zhong, "Enhanced electrical, mechanical and tribological properties of Cu–Cr–Zr alloys by continuous extrusion forming and subsequent aging treatment," Mater. Sci. Technol. **110**, 187–197 (2022).
4. Y. Du, Y. Zhou, K. Song, T. Huang, D. Hui, H. Liu, C. Cheng, J. Yang, L. Niu, and H. Guo, "Zr-containing precipitate evolution and its effect on the mechanical properties of Cu–Cr–Zr alloys," J. Mater. Res. Technol. **14**, 1451–1458 (2021).
5. T. Wang, K. Lu, T. Qiu, X. Zeng, H. Ning, Z. Yang, Y. Li, Q. Ye, R. Yao, and J. Peng, "Highly conductive and adhesive ternary Cu–Cr–Zr alloy electrode for flexible optoelectronic applications," Superlatt. Microstruct. **157**, 106989 (2021).
6. N. R. Bochvar, O. V. Rybalchenko, D. V. Shangina, and S. V. Dobatkin, "Effect of equal-channel angular pressing on the precipitation kinetics in Cu–Cr–Hf alloys," Mater. Sci. Eng. A **757**, 84–87 (2019).
7. G. Purcek, H. Yanar, D. V. Shangina, M. Demirtas, N. R. Bochvar, and S. V. Dobatkin, "Influence of high pressure torsion-induced grain refinement and subsequent aging on tribological properties of Cu–Cr–Zr alloy," J. Alloys Compd. **742**, 325–333 (2018).
8. I. V. Khomskaya, V. I. Zel'dovich, N. Y. Frolova, D. N. Abdullina, and A. E. Kheifets, "Investigation of Cu_5Zr particles precipitation in Cu–Zr and Cu–Cr–Zr alloys subjected to quenching and high strain rate deformation," Lett. Mater. **9** (4), 400–404 (2019).
9. K. Jha, S. Neogy, S. Kumar, R. N. Singh, and G. K. Dey, "Correlation between microstructure and mechanical properties in the age-hardenable Cu–Cr–Zr alloy," J. Nucl. Mater. **546**, 152775 (2021).
10. G. Purcek, H. Yanar, M. Demirtas, D. V. Shangina, N. R. Bochvar, and S. V. Dobatkin, "Microstructural, mechanical and tribological properties of ultrafine-grained Cu–Cr–Zr alloy processed by high pressure torsion," J. Alloys Compd. **816**, 152675 (2020).
11. D. V. Shan'gina, N. I. Ivanov, N. R. Bochvar, and S. V. Dobatkin, "Resistance of the contact welding electrodes made of a Cu–0.7% Cr–0.9% Hf alloy with an ultrafine-grained structure," Russ. Metall. (Metally), No. 9, 815–819 (2018).
12. J. Li, J. Wongsa-Ngam, J. Xu, D. Shan, B. Guo, and T. G. Langdon, "Wear resistance of an ultrafine-grained Cu–Zr alloy processed by equal-channel angular pressing," Wear. **326–327**, 10–19 (2015).
13. Yu. S. Radyuchenko, *Rotary Swaging* (Mashgiz, Moscow, 1962).
14. O. K. Dedyulina and G. A. Salishchev, "Formation of an ultrafine-grained structure in the 40KhGNM medium-carbon steel by rotary swaging and its effect on mechanical properties," Fundam. Issled., Nos. 1–3, 701–706 (2013).
15. Y. Estrin, N. Martynenko, E. Lukyanova, V. Serebryany, M. Gorshenkov, M. Morozov, V. Yusupov, and S. Dobatkin, "Effect of rotary swaging on microstructure, texture, and mechanical properties of a Mg–AlZn alloy," Advanc. Eng. Mater. **22** (1), 1900506 (2020).
16. N. R. Bochvar, O. V. Rybalchenko, N. P. Leonova, N. Yu. Tabachkova, G. V. Rybalchenko, and L. L. Rokhlin, "Effect of cold plastic deformation and subsequent aging on the strength properties of $AlMg_2Si$ alloys with combined (Sc + Zr) and (Sc + Hf) additions," J. Alloys Compd. **821**, 153426 (2020).
17. A. Meng, X. Chen, J. Nie, L. Gu, Q. Mao, and Y. Zhao, "Microstructure evolution and mechanical properties of commercial pure titanium subjected to rotary swaging," J. Alloys Compd. **859**, 158222 (2021).
18. A. H. Huang, Y. F. Wang, M. S. Wang, L. Y. Song, Y. S. Li, L. Gao, C. X. Huang, and Y. T. Zhu, "Optimizing the strength, ductility and electrical conductivity of a Cu–Cr–Zr alloy by rotary swaging and aging treatment," Mater. Sci. Eng. A **746**, 211–216 (2019).

Translated by T. Gapontseva